Calibration of Scanning Electron Microscope using a multi-image non-linear minimization process

Le Cui[1] and Eric Marchand[2]

Abstract— **In this paper, a novel approach of SEM calibration based on non-linear minimization process is presented. The SEM calibration for the intrinsic parameters are achieved by an iterative non-linear optimization algorithm which minimize the registration error between the current estimated position of the pattern and its observed position. The calibration can be achieved by one image and multiple images of calibration pattern. Perspective and parallel projection models are addressed in this approach. The experimental results show the efficiency and accuracy of the proposed method.**

I. INTRODUCTION

Scanning electron microscope (SEM) is an electron microscope where a focused beam of electrons is used to scan the surface of a specimen. This is an essential instrument to display, measure and manipulate the micro and nano-structure with a micrometers or nanometers accuracy. When the task requires the computation of metric information from the acquired 2D images, the calibration of the SEM is an important issue to be considered.

Since the structure of a scanning electron microscope is very different from the structure of an optical microscope, it became apparent that novel image analysis, geometrical projection models and calibration processes would be necessary in order to extract accurate information from the SEM images. In earlier studies, photogrammetric analysis of SEM has been considered by several authors [1],[6]. The projection model relates a three-dimensional (3D) point on a specimen in the observed space to its projection in the two-dimensional (2D) image. Previous studies consider that at low magnification, perspective projection model can be applied because the observed area and electron beam sweep angle are both large. At higher magnification, the center of projection is usually regarded at infinity so the parallel projection model is assumed. However, the practical limit between the choice of perspective projection and parallel projection model is not clear. Some experiments [4],[16] show that parallel projection is assumed at magnification of $1000\times$ and higher. [9] have concluded that the use of parallel projection depends on the desired accuracy for the calculation of position of a point on the specimen. Another important issue in calibration is distortion, which contains spatial distortion (static distortion) and time-dependent drift (temporally-varying distortion). The drift is mainly due to the accumulation of electrons on the surface of the observed specimen. In this paper, we assume that it is compensated by [17]. Several papers [11],[16] ignore distortion and consider only a pure projection model. A few authors [6],[8] consider this with parametric models. Spatial distortion including radial distortion and spiral distortion are introduced in their geometric model. In [4], the distortion removal function is determined before the calibration stage. In this method, good guesses are required in the measurement to ensure the accuracy. Recently, a landmark-based 3D calibration strategy [15] is proposed applying a 3D micrometre-sized reference structure with the shape of a cascade slope-step pyramid. The fabrication of this special 3D reference structure is an important issue. Since different scales of magnification are needed in some applications, [13] considers the modeling magnification-continuous parameters of the static distortion and the projection of the SEM.

In this paper, we address the mentioned calibration problems of SEM: projection models and spatial distortions. A novel approach of SEM calibration involving a full scale non-linear optimization is proposed. The pose (ie, position and orientation of the calibration pattern frame in the sensor frame) computation and SEM calibration are considered simultaneously. The formulation is simple and versatile. An iterative algorithm has been developed to acquire accurate results of calibration. The paper is organized as follows. First, geometrical projection model is described in Section II. Section III introduces the principle of calibration process. The experimental results at various magnifications that validate the approach are shown in Section IV.

II. CONSIDERED PROJECTION MODEL FOR A SEM

In this paper we shall focus on the geometrical calibration of the system projection model. Our final goal is to achieve visual servoing tasks for object positioning and manipulation. Therefore for simplicity issues we decide to consider classical projection models. Whereas such model as a clear physical meaning when considering optical devices, this is no longer the case with a SEM. Nevertheless, for the targeted applications, considering classical projection model has proved to be sufficient [6] (such assertion may no longer be true for, eg, structure characterization). It is however important to determine the nature of the projection model to be considered: parallel and perspective models.

The goal of the calibration process is to determine the set of parameters which define the relationship between the 3D coordinates of an object point on the observed specimen and its projection in the image plane (such parameters that include, in an optical system, the focal length, the dimension

[1]Le Cui is with Université Rennes 1, Lagadic team, IRISA, Rennes, France le.cui@univ-rennes1.fr

[2]Eric Marchand is with Université Rennes 1, Lagadic team, IRISA, Inria Rennes, France eric.marchand@irisa.fr

of pixel, the location of principle points on the image plan are named intrinsic parameters).

Previous studies [8],[9] propose to consider two projection models: perspective projection (central projection) and parallel projection (typically orthographic projection). The perspective projection, where objects are projected towards a point referred to as the center of projection, is widely used in classical camera models, such as the pinhole camera and the digital camera. The parallel projection corresponds to a perspective projection with an infinite focal length. The projection rays and the image plane is perpendicular in parallel projection model. We shall consider these two models within a multi-image non-linear calibration process.

A. Perspective projection

Let ${}^c\mathbf{X} = ({}^cX, {}^cY, {}^cZ, 1)$ be the coordinates of a point on the observed object expressed in the sensor frame (located on the projection center). $\boldsymbol{x} = (x, y, 1)$ is the coordinates of its projection in the image plane expressed in normalized coordinate (ie, in meter). We have [12]

$$\begin{cases} x = \dfrac{{}^cX}{{}^cZ} \\ \\ y = \dfrac{{}^cY}{{}^cZ} \end{cases} \tag{1}$$

leading in the actual image coordinates expressed in pixel $\boldsymbol{x}_p = (u, v)$ on the image plane and given by

$$\begin{cases} u = u_0 + p_x x \\ v = v_0 + p_y y \end{cases} \tag{2}$$

where p_x and p_y represent the pixel/meter ratio and u_0, v_0 the principal point coordinates in the image plane. According to (1) and (2), the general expression of perspective projection is:

$$\begin{bmatrix} u \\ v \\ 1 \end{bmatrix} = \begin{bmatrix} p_x & 0 & u_0 \\ 0 & p_y & v_0 \\ 0 & 0 & 1 \end{bmatrix} \begin{bmatrix} 1 & 0 & 0 & 0 \\ 0 & 1 & 0 & 0 \\ 0 & 0 & 1 & 0 \end{bmatrix} \begin{bmatrix} {}^cX \\ {}^cY \\ {}^cZ \\ 1 \end{bmatrix}. \tag{3}$$

In a camera calibration in perspective projection model, p_x, p_y, u_0 and v_0 are intrinsic parameters.

B. Parallel projection

In parallel projection model, the projection rays are parallel. The coordinates of a 2D point $\boldsymbol{x} = (x, y)$ corresponds to its 3D coordinates ${}^c\mathbf{X} = ({}^cX, {}^cY, {}^cZ)$:

$$\begin{cases} x = {}^cX \\ y = {}^cY \end{cases} \tag{4}$$

leading to position $\boldsymbol{x}_p = (u, v)$ in the digital image is

$$\begin{cases} u = p_x x \\ v = p_y y \end{cases}. \tag{5}$$

According to (4) and (5), the general expression of parallel projection can be written as

$$\begin{bmatrix} u \\ v \end{bmatrix} = \begin{bmatrix} p_x & 0 \\ 0 & p_y \end{bmatrix} \begin{bmatrix} 1 & 0 & 0 \\ 0 & 1 & 0 \end{bmatrix} \begin{bmatrix} {}^cX \\ {}^cY \\ {}^cZ \end{bmatrix}. \tag{6}$$

Since there is no longer principle point in parallel projection, only p_x and p_y are considered as the intrinsic parameters.

C. Image distortion

In classical models [7], the most commonly used spatial distortion is radial distortion. Considering the distortion, the relation between the pixel position $\boldsymbol{x}$ and the coordinates in the image plane $\boldsymbol{x}_p$ in perspective projection is expressed by

$$\begin{cases} u = u_0 + p_x x + \delta_u \\ v = v_0 + p_y y + \delta_v \end{cases}. \tag{7}$$

The radial distortion can be approximated using

$$\begin{cases} \delta_u = \tilde{u}(k_1 r^2 + k_2 r^4 + ...) \\ \delta_v = \tilde{v}(k_1 r^2 + k_2 r^4 + ...) \end{cases} \tag{8}$$

where $r^2 = \tilde{u}^2 + \tilde{v}^2$, $\tilde{u} = u - u_0$ and $\tilde{v} = v - v_0$. Usually, to compensate for the radial distortion, one or two coefficients are enough. It has to be noted that in SEM image such distortion appears to be very small.

Another issue that can be considered is the skewness between the x- and y-axis. In this case we have:

$$\begin{cases} u = u_0 + p_x x + \gamma y \\ v = v_0 + p_y y \end{cases}. \tag{9}$$

Typically, γ is null when the pixel in x- and y-axis is exactly rectangular.

In [10], the spiral distortion is caused by the spiral of the electrons within the microscope column. It is usually given by

$$\begin{cases} u = u_0 + p_x(x + \delta_x) \\ v = v_0 + p_y(y + \delta_y) \end{cases} \tag{10}$$

where $\delta_x = s_1(x^2 y + y^3)$, $\delta_y = s_2(x^3 + xy^2)$, s_1 and s_2 are spiral coefficients.

In the parallel model, the distortion models is similar but u_0 and v_0 are null in equation (7), (9) and (10).

III. Non-linear calibration process

Calibration is an old research area that received much attention since the early 70's, first in the photogrammetry community (eg, [2]) then in the computer vision and robotics communities (eg, [5], [18], [19], etc.). Most of the approaches consider the calibration issue as a registration problem that consists in determining the relationship between 3D coordinates of points and their 2D projections in the image plane. These 3D features are usually a part of a calibration pattern (sometime a 3D calibration rig) and the position of these features in a world frame have to be known with a very good accuracy. Performing the calibration leads to the estimation of the intrinsic camera parameters (image center, focal length, distortion) but also, as a by-product, extrinsic camera parameters (ie, the pose).

Various techniques exist to achieve the calibration. Among these techniques, full-scale non-linear optimization techniques (introduced within the photogrammetry community [2]) have proved to be very efficient. They consist in minimizing the error between the observation and the back-projection of the model. Minimization is handled using

numerical iterative algorithms such as Newton-Raphson or Levenberg-Marquartd.

A. Calibration

As stated the goal is to minimize the error between points extracted from the image $\boldsymbol{x}_p^*$ and the projection of the model of the calibration pattern for given model parameters (both intrinsic parameters and pose) $\boldsymbol{x}_p(\mathbf{r}, \xi)$.

We define the error $\Delta = \mathbf{e}^\top \mathbf{e}$ between the desired state of image feature $\boldsymbol{x}_p^*$ and the current state $\boldsymbol{x}_p(\mathbf{r}, \xi)$:

$$\mathbf{e} = \boldsymbol{x}_p(\mathbf{r}, \xi) - \boldsymbol{x}_p^* \tag{11}$$

where $\boldsymbol{x}_p(\mathbf{r}, \xi)$ is computed using equation (2) or (5). To minimize this cost function, we specify an exponential decrease of the error:

$$\dot{\mathbf{e}} = -\lambda \mathbf{e} \tag{12}$$

where λ is a proportional coefficient. In (12), $\dot{\mathbf{e}}$ can be simply computed from the time variation of $\dot{\boldsymbol{x}}_p$ which is given by:

$$\dot{\boldsymbol{x}}_p = \frac{\partial \boldsymbol{x}_p}{\partial \mathbf{r}} \frac{d\mathbf{r}}{dt} + \frac{\partial \boldsymbol{x}_p}{\partial \xi} \frac{d\xi}{dt} \tag{13}$$

where $\mathbf{r}$ represent the (virtual) sensor position along the minimization trajectory (translation and rotation), $\mathbf{v} = \dfrac{d\mathbf{r}}{dt}$ is the sensor velocity during the minimization. Rewrite (13):

$$\dot{\boldsymbol{x}}_p = \mathbf{J}_p \mathbf{V} \tag{14}$$

where $\mathbf{V} = \begin{bmatrix} \mathbf{v} \\ \dot{\xi} \end{bmatrix}$. Matrix $\mathbf{J}_p$ is the image Jacobian, it is given by:

$$\mathbf{J}_p = \begin{bmatrix} \dfrac{\partial \boldsymbol{x}_p}{\partial \mathbf{r}} & \dfrac{\partial \boldsymbol{x}_p}{\partial \xi} \end{bmatrix}. \tag{15}$$

Combining (14) and (12), we finally get:

$$\mathbf{V} = -\lambda \mathbf{J}_p^+ (\boldsymbol{x}_p(\mathbf{r}, \xi) - \boldsymbol{x}_p) \tag{16}$$

where $\mathbf{J}_p^+$ is the pseudo inverse of matrix $\mathbf{J}_p$ and $\mathbf{V}$ being the parameters increment computed at each iteration of this minimization process.

B. Multi-image calibration

In practice, the intrinsic parameters are usually obtained by different viewpoints of the calibration pattern from the same camera. The optimization scheme requires the computation of the position of calibration pattern and a common set of intrinsic parameters. In that case the global error to be minimized is given by

$$\Delta = \sum_{i=1}^{n} (\mathbf{e}_i^\top \mathbf{e}_i) \tag{17}$$

with

$$\mathbf{e}_i = \boldsymbol{x}_p(\mathbf{r}_i, \xi) - \boldsymbol{x}_p^* \tag{18}$$

Let $\boldsymbol{x}_p^i$ be a set of images features extracted from the i^{th} image. In multi-image calibration, rewrite (14):

$$\begin{bmatrix} \dot{\boldsymbol{x}}_p^1 \\ \dot{\boldsymbol{x}}_p^2 \\ \vdots \\ \dot{\boldsymbol{x}}_p^n \end{bmatrix} = \mathbf{J}_p \begin{bmatrix} \mathbf{v}^1 \\ \mathbf{v}^2 \\ \vdots \\ \mathbf{v}^n \\ \dot{\xi} \end{bmatrix} \tag{19}$$

with

$$\mathbf{J}_p = \begin{bmatrix} \dfrac{\partial \boldsymbol{x}_p^1}{\partial \mathbf{r}} & 0 & \cdots & 0 & \dfrac{\partial \boldsymbol{x}_p^1}{\partial \xi} \\ 0 & \dfrac{\partial \boldsymbol{x}_p^2}{\partial \mathbf{r}} & 0 & 0 & \dfrac{\partial \boldsymbol{x}_p^2}{\partial \xi} \\ \vdots & \vdots & \ddots & \vdots & \vdots \\ 0 & \cdots & 0 & \dfrac{\partial \boldsymbol{x}_p^n}{\partial \mathbf{r}} & \dfrac{\partial \boldsymbol{x}_p^n}{\partial \xi} \end{bmatrix}. \tag{20}$$

C. Nonlinear optimization

In the nonlinear minimization process, the optimization algorithm is an important issue. The general idea of minimizing a nonlinear function is to successively update the parameters such that the value of cost function decreases at each iteration as specified by equation (12). The Gauss-Newton method is usually used in nonlinear optimization as presented in equation (16).

Particularly, the measured values are small in the SEM imaging (point coordinates are expressed in micrometer (μm) and nanometer (nm)). Several numerical problems are then induced into the optimization algorithms. For example, these tiny values causes rank deficiency of Jacobian matrix $\mathbf{J}_p$. Sometimes the computation of equation (16) is impossible. In this case, the Levenberg-Marquardt method is considered:

$$\mathbf{V} = -\lambda (\mathbf{J}_p^\top \mathbf{J}_p + \mu \mathbf{I})^{-1} \mathbf{J}_p^\top \mathbf{e} \tag{21}$$

where I is a identity matrix and μ is a coefficient whose typical value ranges from 0.001 or 0.0001. With modifying μ, the algorithm is set to adapt the input data and to avoid numerical problems.

D. Jacobian

In this paper, the computation of $\dfrac{\partial \boldsymbol{x}_p}{\partial \mathbf{r}}$ and $\dfrac{\partial \boldsymbol{x}_p}{\partial \xi}$ in the interaction matrix $\mathbf{J}_p$ is presented with the two specified projection models above.

The image Jacobian $\dfrac{\partial \boldsymbol{x}_p}{\partial \mathbf{r}}$ relates the motion of a point in the image to the (virtual) sensor motion, it could be expressed by:

$$\frac{\partial \boldsymbol{x}_p}{\partial \mathbf{r}} = \begin{bmatrix} p_x & 0 \\ 0 & p_y \end{bmatrix} \mathbf{L}. \tag{22}$$

1) Perspective projection: In the perspective projection model, the Jacobian is $\mathbf{L}$ is given by [3]:

$$\mathbf{L} = \begin{bmatrix} -\dfrac{1}{Z} & 0 & \dfrac{x}{Z} & xy & -(1+x^2) & y \\ 0 & -\dfrac{1}{Z} & \dfrac{y}{Z} & 1+y^2 & -xy & -x \end{bmatrix}. \tag{23}$$

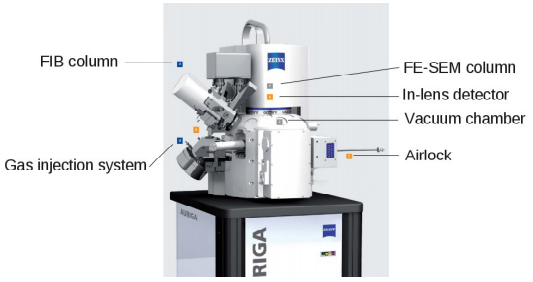

Fig. 1. Carl Zeiss AURIGA SEM

From (2), without considering the distortion in the camera model, the deviation of image feature $\boldsymbol{x}_p$ by intrinsic parameters ξ is:

$$\frac{\partial \boldsymbol{x}_p}{\partial \xi} = \begin{bmatrix} x & 0 & 1 & 0 \\ 0 & y & 0 & 1 \end{bmatrix}. \tag{24}$$

If we consider one coefficient k in radial distortion (k_1 in (8)), the skew factor γ and spiral coefficient s_1, s_2 as distortion parameters, the deviation of image feature $\boldsymbol{x}_p$ by intrinsic parameters ξ with distortion factors is:

$$\frac{\partial \boldsymbol{x}_p}{\partial \xi} = \begin{bmatrix} x + s_1(x^2y + y^3) & 0 \\ 0 & y + s_2(x^3 + xy^2) \\ 1 - k(r^2 + 2\tilde{u}^2) & -2k\tilde{u}\tilde{v} \\ -2k\tilde{u}\tilde{v} & 1 - k(r^2 + 2\tilde{v}^2) \\ \tilde{u}r^2 & \tilde{v}r^2 \\ y & 0 \\ p_x(x^2y + y^3) & 0 \\ 0 & p_y(x^3 + xy^2) \end{bmatrix}^\top. \tag{25}$$

2) Parallel projection: With a parallel projection model, the Jacobian is given by:

$$\mathbf{L} = \begin{bmatrix} -1 & 0 & 0 & 0 & -Z & y \\ 0 & -1 & 0 & Z & 0 & -x \end{bmatrix}. \tag{26}$$

Comparing with equation (23), it is evident that the motion along the Z axis is not observable. Therefore the depth of the calibration pattern cannot be recovered. The deviation $\frac{\partial \boldsymbol{x}_p}{\partial \xi}$ without distortion is given from (5):

$$\frac{\partial \boldsymbol{x}_p}{\partial \xi} = \begin{bmatrix} x & 0 \\ 0 & y \end{bmatrix}. \tag{27}$$

With distortion, it is expressed:

$$\frac{\partial \boldsymbol{x}_p}{\partial \xi} = \begin{bmatrix} x & 0 & \tilde{u}r^2 & y & p_x(x^2y + y^3) & 0 \\ 0 & y & \tilde{v}r^2 & 0 & 0 & p_y(x^3 + xy^2) \end{bmatrix}. \tag{28}$$

IV. Experimental results

The SEM microscope that has been used to validate the developed calibration method is a Carl Zeiss AURIGA 60 (Fig. 1). It provides a wide magnification ranges from 12× to 1000k×. Within the SEM a 6DoF platform is available, including 360° continuous rotation and tilt from -15° to 70°.

A multi-scale planar calibration pattern (see Fig. 2) is used in the calibration procedure. It is a hierarchy of chessboard

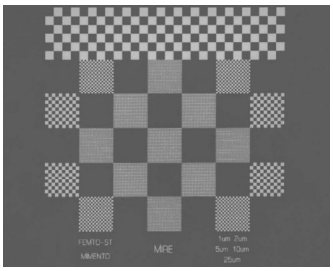

Fig. 2. Multi-scale calibration planar, square size from 1μm up to 25 μm

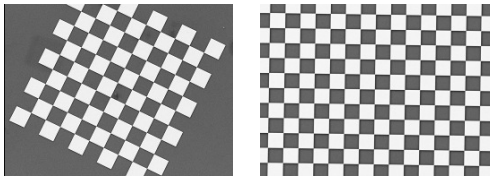

(a) (b)

Fig. 3. Calibration images (a)800× with 20°rotation (b)1500× with 4°tilt

grids where size of each square are of 25 μm, 10μm, 5μm, 2μm and 1μm. Acquired image size is 1024×768 pixels. Several sets of calibration images (Fig. 3) have been acquired within the SEM with different magnifications ranging 300× up to 10k×. Each group (with a given magnification) contents 7 to 9 images of the pattern acquired from various poses with rotation around Z axis ranging from 0° to 40°, and tilt from 0° to 8°.

The proposed calibration procedure has been implemented with the ViSP library [14]. Considering the chessboard shape of our calibration pattern, we have used the OpenCV chessboard corners detector in order to obtain a precise localization of each corner. A linear algorithm has been considered to have a first approximation of the calibration parameters [20]. The multi-image iterative non-linear minimization method for calibration, using both perspective and projection model, is then used. The intrinsic parameters are then computed by minimizing the residual error between the projection of the pattern for the current estimated pose and the observed one.

A. Minimization process and algorithm behavior

To illustrate the behavior and performance of the proposed algorithm, we consider here the calibration of the SEM using a parallel projection model and without adding any distortion parameters.

In this experiment, the SEM magnification has been set to 2000×, the size of each pattern square is of 5μm. Eight images of the calibration pattern have been acquired from eight poses with rotation from 0° up to 20° and tilt from 0° up to 8° and used in the calibration process. The gain λ in equation (12) in the algorithm is set to 0.4. Fig. 4(a) shows the residual error computed at each iteration of the minimization process. The evolution of intrinsic parameters p_x and p_y is shown in Fig. 4(b). The residual error and the intrinsic parameters converge quickly even thought the value

TABLE I

CALIBRATION ON PERSPECTIVE AND PARALLEL PROJECTION

magnification	Perspective projection						Parallel projection		
	p_x	p_y	u_0	v_0	$Z_1(\mu m)$	$\|\mathbf{e}\|$	p_x(pixel/μm)	p_y(pixel/μm)	$\|\mathbf{e}\|$
500	70168.0	70058.3	511.4	384.1	15752.7	0.15	4.47	4.44	0.38
1000	201505.3	199729.8	511.6	384.4	22302.1	0.08	8.98	8.96	0.20
2000	122073.3	122312.0	511.5	384.3	6803.4	0.12	17.96	18.10	0.16
5000	103917.4	105067.7	511.5	384.0	2316.2	0.23	44.86	45.50	0.24

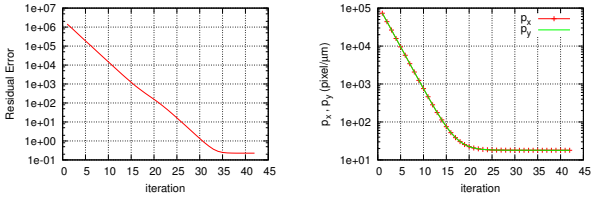

(a) (b)

Fig. 4. Evolution of (a) residual error in pixel and (b) intrinsic parameters p_x and p_y during the minimization process

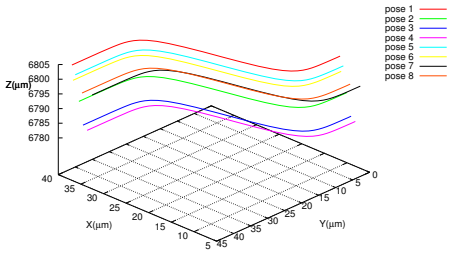

Fig. 5. Estimated target positions during the minimization process

is significant at the beginning. Only a few iterations less than 50 are required by the process. Fig. 5 presents the estimated set of extrinsic parameters (estimated sensor poses) during the minimization process. It can be noted that, as expected, motion along the Z axes is not observable using the parallel projection model (in equation (26), the elements in the third column of the interaction matrix which corresponds to the Jacobian of translation on Z axis are indeed null).

B. Projection models

Another experiment aims to test two projection models that can be possibly considered for the calibration of a SEM. To compare the performance with different scales, four magnifications are considered: 500×, 1000×, 2000× and 5000×. Note that it is suggested in the literature [4],[16] that perspective projection can be applied for a magnification up to 1000× whereas parallel projection should be considered for higher magnification. Table I shows the estimated calibrated intrinsic parameters p_x, p_y, u_0 and v_0, the estimated distance Z_1 between sensor and calibration pattern (for the first image) and the residual error $\|\mathbf{e}\|$ in pixel. In all the case the algorithm converges and the registration error is less than 0.5 pixel per point which correspond to the noise level in corner extraction. It is quite clear from the estimation of parameters p_x and p_y that, with the perspective projection model, intrinsic parameters are inconsistent. Nevertheless the ratio $p_x/(Z_1 M)$ is almost constant (see Table II) which confirms the fact that the difference between p_x (or p_y) and object depth is not observable. This motivates the choice of the parallel projection model for future visual servoing experiments despite the fact that depth motion are not observable.

Table II shows the $p_{(x,y)}/(Z_1 M)$ for perspective projection and $p_{(x,y)}/M$ for parallel projection. These factors are approximately a constant value in the two projection models.

TABLE II

RELATION BETWEEN PIXEL SIZE AND DEPTH FOR VARIOUS MAGNIFICATION: $p_{(x,y)}/(Z_1 M)$ FOR PERSPECTIVE PROJECTION AND $p_{(x,y)}/M$ FOR PARALLEL PROJECTION

magnification M	500	1000	2000	5000
$p_x/(Z_1 M)$	0.00890	0.00903	0.00897	0.00897
$p_y/(Z_1 M)$	0.00889	0.00895	0.00898	0.00907
p_x/M	0.00895	0.00898	0.00898	0.00897
p_y/M	0.00888	0.00895	0.00904	0.00910

We have tested a wide range of magnifications from 300× to 10k× considering parallel projection model. Results are shown in Table III. The intrinsic parameters through magnifications are shown in Fig. 6. The ratio between the computed intrinsic parameters p_x, p_y and magnification M is almost constant: as expected a quasi linear relation exists between p_x, p_y and magnification as shown in Fig. 6. It as to be noted that the residual error $\|\mathbf{e}\|$ is slightly more important for low magnification meaning that parallel projection model is less appropriate at low magnification (300×, 500×) which confirms earlier report [16]. $\|\mathbf{e}\|$ also increases at high magnification but the reason is that at high magnification the extraction of corner position on the calibration pattern used in our experiment could not be as accurate as that at low magnification.

C. Distortion issues

Finally, an experiment has been realized to test the potential effects of distortion. Three magnifications are considered in this experiments: 500×, 2000× and 5000×. To compare the performance of calibration with and without distortion parameters, all the factors (gain, coefficient in Levenberg-Marquardt optimization, etc.) in the algorithm are fixed. Table IV shows the calibrated radial distortion parameter k, skewness parameter γ, intrinsic parameters p'_x, p'_y, residual error $\|\mathbf{e}'\|$ with distortion and intrinsic parameters p_x, p_y, residual error $\|\mathbf{e}\|$ without distortion. Results are obtained on parallel projection model. It is evident that introducing

TABLE III

CALIBRATION ON PARALLEL PROJECTION WITH RESPECT TO MAGNIFICATION

magnification M	300	500	800	1000	1500	2000	5000	10 000
p_x (pixel/μm)	2.69	4.47	7.20	8.98	13.43	17.96	44.86	89.81
p_y (pixel/μm)	2.72	4.44	7.32	8.96	13.91	18.09	45.50	89.76
$\|\mathbf{e}\|$	0.51	0.38	0.27	0.19	0.13	0.16	0.24	0.41
p_x/M	0.00897	0.00895	0.00900	0.00895	0.00895	0.00898	0.00897	0.00898
p_y/M	0.00909	0.00889	0.00915	0.00895	0.00927	0.00904	0.00910	0.00897

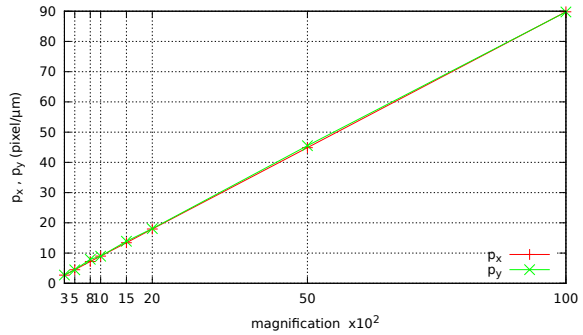

Fig. 6. Intrinsic parameters with respect to magnification scales

distortion parameters does not affect the computation of the main intrinsic parameters p_x, p_y and does not improve the residual error. In this case, such spatial distortion could be typically ignored in the calibration process.

TABLE IV

CALIBRATION WITH/WITHOUT DISTORTION

	magnification		
	500	2000	5000
k	-5.65×10^{-9}	-3.67×10^{-10}	-1.15×10^{-10}
γ	0.0024	0.0033	0.0061
s_1	8.64×10^{-7}	-1.28×10^{-7}	-2.87×10^{-7}
s_2	7.19×10^{-6}	2.79×10^{-7}	9.68×10^{-6}
p'_x (pixel/μm)	4.46	17.96	44.87
p'_y (pixel/μm)	4.46	18.00	45.36
$\|\mathbf{e}'\|$	0.57	0.23	0.27
p_x (pixel/μm)	4.46	17.97	44.86
p_y (pixel/μm)	4.46	18.00	45.37
$\|\mathbf{e}\|$	0.57	0.23	0.26

V. CONCLUSIONS

In this paper, a simple and efficient method of SEM calibration has been addressed. A global multi-image non-linear minimization process that minimizes the residual error between the projection of the calibration pattern and its observation in the image was considered. The precise intrinsic parameters as well as the position of the sensor with respect to the pattern are computed. The choice of the parallel projection model has been validated for SEM images. The spatial distortion parameters (skewness, radial distortion and spiral distortion) are such insignificant in our experiments that can be eliminated.

ACKNOWLEDGMENT

The author wish to thank Naresh Marturi and Sounkalo Dembélé for the calibration images acquired at FEMTO-ST laboratory in Besançon, France. This work was realized in the context of the French ANR P2N Nanorobust project.

REFERENCES

[1] A. Boyde. Quantitative photogrammetric analysis and qualitative stereoscopic analysis of sem images. *Journal of Microscopy*, 98(3):452–471, 1973.

[2] D.C. Brown. Close-range camera calibration. *Photogrammetric Engineering*, 4(2):127–140, March 1971.

[3] A.I. Comport, E. Marchand, M. Pressigout, and F. Chaumette. Real-time markerless tracking for augmented reality: the virtual visual servoing framework. *IEEE Trans. on Visualization and Computer Graphics*, 12(4):615–628, July 2006.

[4] N. Cornille, D. Garcia, M.A. Sutton, S. McNeill, and J. Orteu. Automated 3-d reconstruction using a scanning electron microscope. In *SEM annual conf. & expo. on exp. & app. mech.*, 2003.

[5] O.D Faugeras and G. Toscani. Camera calibration for 3D computer vision. In *Proc Int. Workshop on Machine Vision and Machine Intelligence*, pages 240–247, Tokyo, February 1987.

[6] S.K. Ghosh. Photogrammetric calibration of a scanning electron microscope. *Photogrammetria*, 31(3):91 – 114, 1975.

[7] J. Heikkila and O. Silven. A four-step camera calibration procedure with implicit image correction. In *Proc. of IEEE Conf. on Computer Vision and Pattern Recognition*, pages 1106–1112, 1997.

[8] M. Hemmleb and J. Albertz. Microtopography-the photogrammetric determination of friction surfaces. *International Archives of Photogrammetry and Remote*, 33:56–63, 2000.

[9] P.G.T. Howell. A theoretical approach to the errors in sem photogrammetry. *Scanning*, 1(2):118–124, 1978.

[10] O. Klemperer and M. E. Barnett. *Electron optics*. Cambridge University Press, Cambridge, U.K., 1971.

[11] A.J. Lacey, N.A. Thacker, and R.B. Yates. Surface approximation from industrial sem images. In *British Machine Vision Conference*, pages 725–734, 1996.

[12] Y. Ma, S. Soatto, J. Košecká, and S. Sastry. *An invitation to 3-D vision*. Springer, 2004.

[13] A. C. Malti, S. Dembélé, N. Le Fort-Piat, P. Rougeot, and R. Salut. Magnification-continuous static calibration model of a scanning-electron microscope. *J. of Electronic Imaging*, 21(3):033020–1, 2012.

[14] E. Marchand, F. Spindler, and F. Chaumette. Visp for visual servoing: a generic software platform with a wide class of robot control skills. *IEEE Robotics & Automation Magazine*, 12(4):40–52, 2005.

[15] M. Ritter, M. Hemmleb, B. Lich, P. Faber, and H. Hohenberg. Sem/fib stage calibration with photogrammetric methods. In *ISPRS Commission V Symp. 2006 (Int. Archives of Photogrammetry, Remote Sensing and Spatial Information Sciences)*, volume 36, 2006.

[16] O. Sinram, M. Ritter, S. Kleindick, A. Schertel, H. Hohenberg, and J. Albertz. Calibration of an sem, using a nano positioning tilting table and a microscopic calibration pyramid. *Int. Arch. Photogramm. Remote Sens. Spatial Inf. Sci.*, 34(5):210–215, 2002.

[17] M.A. Sutton, N. Li, D. Garcia, N. Cornille, J. Orteu, S.R. McNeill, H.W. Schreier, and X. Li. Metrology in a scanning electron microscope: theoretical developments and experimental validation. *Measurement Science and Technology*, 17(10):2613, 2006.

[18] R.Y. Tsai. A versatile camera calibration technique for high-accuracy 3D machine vision metrology using off-the-shelf tv cameras and lenses. *IEEE J. of Robotics and Automation*, 3(4):323–344, 1987.

[19] J. Weng, P. Cohen, and N. Rebiho. Motion and structure estimation from stereo image sequences. *IEEE Trans. on Robotics and Automation*, 8(3):362–382, June 1992.

[20] Z. Zhang. A flexible new technique for camera calibration. *Pattern Analysis and Machine Intelligence, IEEE Transactions on*, 22(11):1330–1334, 2000.